LASER INTERFEROMETER GRAVITATIONAL WAVE OBSERVATORY
-LIGO-
CALIFORNIA INSTITUTE OF TECHNOLOGY
MASSACHUSETTS INSTITUTE OF TECHNOLOGY

**Technical Note** **LIGO-T030290- 00- D** **12/30/03**

# Description of the Angular Sensing and Control (ASC) system in $H_1$ during the third LIGO Science Run (S3)

Luca Matone, Paul Schwinberg, Stefan Ballmer, Matt Evans, Peter Fritschel, Nergis Mavalvala, Virginio Sannibale, Rick Savage, Daniel Sigg

This is an internal working note
of the LIGO Project.

**California Institute of Technology**
**LIGO Project – MS 51-33**
**Pasadena CA 91125**
Phone (626) 395-2129
Fax (626) 304-9834
E-mail: info@ligo.caltech.edu

**Massachusetts Institute of Technology**
**LIGO Project – MS 20B-145**
**Cambridge, MA 01239**
Phone (617) 253-4824
Fax (617) 253-7014
E-mail: info@ligo.mit.edu

WWW: http://www.ligo.caltech.edu

File c:\Work\documents\ASC\T030290-00-D – printed December 30th, 2003

## ABSTRACT

This technical note summarizes the state of the Angular Sensing and Control (ASC) subsystem for $H_1$ during the third LIGO science run (S3). The optical sensing matrix with respect to the angular degrees of freedom, the control matrix, the different noise contributions and photodiode beam centering issues will be addressed.


## INTRODUCTION

The detector's sensitivity deteriorates with

- misalignments of the Test Masses (TM) (decrease of the circulating power, increase of contrast defect, increase of shot-noise, … );
- beam miss centering (angle-to-length coupling).

For these reasons, the residual angular fluctuations of the TMs need to be $10^{-8}$ rad-rms with respect to cavity axis, the sensing noise needs to be $<10^{-14}$ rad/rHz for f>40Hz (WFS1) and the beam spot needs to be centered on the TM to within 1mm (see T980064 for details).

This document describes the ASC subsystem in the 4km long IFO ($H_1$) during S3 (the sub-system in $H_2$ is not as advanced so we will focus mainly on $H_1$). We will first discuss the response of the Wave-Front Sensors (WFSs) to the different angular degrees of freedom (DOF) with their sensing noise. The control topology will then be addressed with its current limitations. The angular noise contribution to the sensitivity curve will be shown and issues about beam positioning on the WFS head will be addressed.

## WAVE-FRONT SENSORS

Any cavity misalignments with respect to the input laser beam couple to higher order transverse modes (TEM). To align the machine, we would like to detect and correct for the amount of higher order modes circulating in the IFO (to first-order approximation, this consists of a combination of TEM01 and TEM10 modes). In order to generate a misalignment signal, we extend the phase modulation-demodulation technique by making use of

- a pair of sidebands that resonate in the power-recycling cavity (PRC) but not in the arms, and
- a pair of sidebands that do not resonate in the PRC.

We then collect the light beams at the Anti-Symmetric (AS) port, on reflection (REFL) and the pick-off from ITMX (POX).

The misalignment signals then consist of the interference between the carrier (sideband) TEM00 mode with the sideband (carrier) TEM01 mode. To resolve the amplitude modulation at the modulation frequency we make use of split photodetectors capable of integrating in the half-plane: the up/down and left/right differences generate a *DC* signal that is used to measure the misalignments. The ensemble of the split photodetector and demodulation electronics is referred to as WFS.

Figure 1 shows the position of the 4 WFSs in $H_1$ during S3. With this setup we have 5x2 (5 TMs, pitch and yaw) signals to correct for 5x2 angular DOF (the Beam Splitter (BS) and the input beam pointing (MMT3) alignment are not controlled by the WFSs).

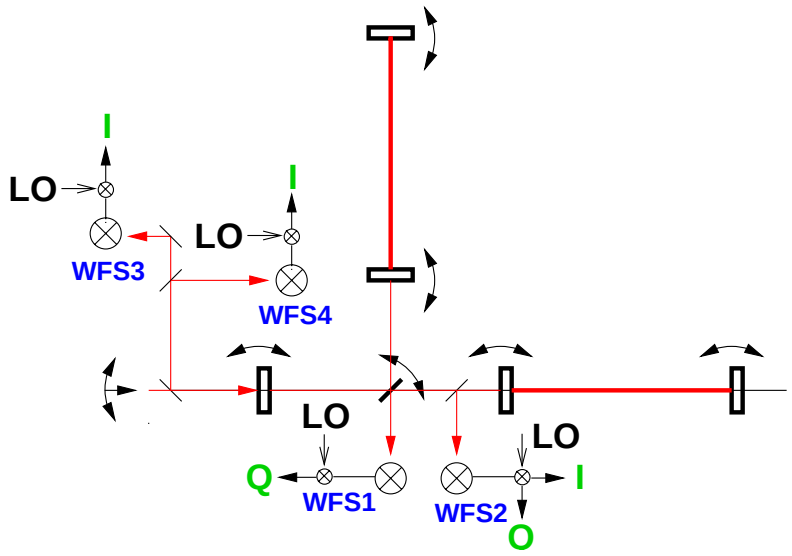


**Figure 1: The location of the different WFSs in $H_1$ during S3.**

The expected misalignment signals are shown in Table 2 (from T980064) where the coefficients are normalized to 1W of light power per misalignment angle (in divergence angle units).

| | Demodulation Phase | Gouy Phase [deg] | ΔETM | ΔITM | <ETM> | <ITM> | RM |
|---|---|---|---|---|---|---|---|
| **WFS1** | **Q** | **90** | **-25.0** | **-11.4** | | | |
| **WFS2A** | **I** | **144** | | | | **0.5** | **-0.7** |
| **WFS2B** | **Q** | **144** | | **-0.1** | | | |
| **WFS3** | **I** | **0** | | | | | **1.9** |
| **WFS4** | **I** | **90** | | | **-2.1** | **-1.0** | |

**Table 1: This is the light power change, normalized to 1W, per misalignment angle normalized by the divergence angle (from T980064, page 15).**

## THE ANGULAR DRIVE CALIBRATIONS

In order to measure the response of the WFSs from the different angular DOF, the IFO needs to be already in a *well* aligned state: arm powers and sideband recycling maximized while minimizing the contrast defect at the dark port. To do this, we close all of the angular control loops and we drive each DOF out of band. To calibrate the WFSs response and the angular control drive in physical units, we make use of the Optical Lever (OL) readings and their calibrations.

Before the beginning of S3, the OLs for $H_1$ and $H_2$ were re-calibrated using fixed reference points. The new calibrations, within 10% of the old ones, are elogged on Oct.9$^{th}$, 2003 by D.Cook.

While using the OLs to calibrate the WFSs, we noticed that non-existent cross-terms would appear in the sensing matrix (cross-terms that would appear only in the calibrated sensing matrix). This originates from a systematic error in the OL calibrations that can be taken into account.

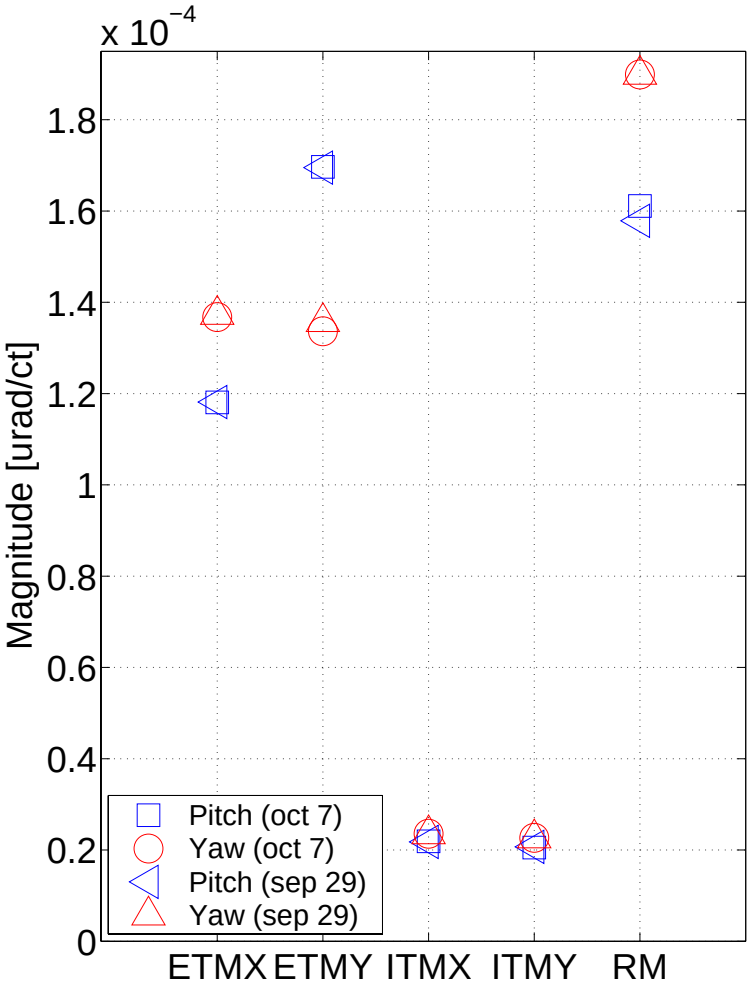


**Figure 1: Calibrated response of the Optical Levers to the different angular DOF measured at 9Hz, pitch/yaw and at different times.**

Figure 1 plots the transfer function magnitude between the calibrated OL reading and the drive (ex. H1:SUS-ETMX_PERROR/H1:SUS-ETMX_ASCPIT_EXC), in pitch and yaw, measured at different times. From the plot we observe that

1. the response is reproducible at the ~1% level;
2. there is a significant systematic difference between the pitch and yaw response (there should be none);
3. there is a significant systematic between the X and Y arms.

The presence of these systematic errors creates significant cross-terms in the calibrated canonical (common-differential base) sensing matrix.

To eliminate the presence of these systematic errors, we use approximated OL responses by taking an average between the pitch/yaw readings and the two arms: we know that we should have an identical pitch/yaw response for each TM, that the X arm optics should respond in the same way as the Y arm optics, and because of the different coil drivers, that the ETM response should be greater than the ITM response by a factor of ~7.

Referring to the data shown in Figure 1, we create the calibration Table 1. The use of this table would allow to estimate the ASC angular drives in physical units in order to keep the IFO in the aligned state.

| Channel name (H1:SUS-) | Calibration @ 9Hz [urad/ct] | Frequency Dependance |
|---|---|---|
| ETMX_ASCPIT(YAW)_EXC<br>ETMX_ASCPIT(YAW)_IN1<br>ETMX_ASCPIT(YAW)_IN2<br>ETMX_P(Y) | 1.4e-4 | (Chebychev 1st type, 8th order 1dB ripple @ 30Hz)*lead*(double pole at 0.5(0.6)Hz) |
| ETMY_ASCPIT(YAW)_EXC<br>ETMY_ASCPIT(YAW)_IN1<br>ETMY_ASCPIT(YAW)_IN2<br>ETMY_P(Y) | 1.4e-4 | (Chebychev 1st type, 8th order 1dB ripple @ 30Hz)*lead*(double pole at 0.5(0.6)Hz) |
| ITMX_ASCPIT(YAW)_EXC<br>ITMX_ASCPIT(YAW)_IN1<br>ITMX_ASCPIT(YAW)_IN2<br>ITMX_P(Y) | 0.2e-4 | Before Nov. 20th, 2003<br>(Chebychev 1st type, 8th order 1dB ripple @ 30Hz)*lead*(double pole at 0.5(0.6)Hz)<br><br>After Nov.20th, 2003<br>(Chebychev 1st type, 8th order 1dB ripple @ 7Hz)*lead*(double pole at 0.5(0.6)Hz) |
| ITMY_ASCPIT(YAW)_EXC<br>ITMY_ASCPIT(YAW)_IN1<br>ITMY_ASCPIT(YAW)_IN2<br>ITMY_P(Y) | 0.2e-4 | Before Nov. 20th, 2003<br>(Chebychev 1st type, 8th order 1dB ripple @ 30Hz)*lead*(double pole at 0.5(0.6)Hz)<br><br>After Nov.20th, 2003<br>(Chebychev 1st type, 8th order 1dB ripple @ 7Hz)*lead*(double pole at 0.5(0.6)Hz) |
| RM_ASCPIT(YAW)_EXC<br>RM_ASCPIT(YAW)_IN1<br>RM_ASCPIT(YAW)_IN2<br>RM_P(Y) | 1.7e-4 | (Chebychev 1st type, 8th order 1dB ripple @ 30Hz)*lead*(double pole at 0.5(0.6)Hz) |

**Table 2: Control channel calibrations; Black denotes Test Point and not saved in Frames; Green denotes channels saved in Frames; 'lead' filter consists of 4 zeros at 100Hz and 4 zeros at 1kHz;**

## THE SENSING MATRIX AND THE CALIBRATED WFS SIGNALS

With an understanding of the actuation chain, we can now address the WFS angular sensing matrix of the subsystem. This matrix was measured by driving at an arbitrary frequency (9Hz in our case) each TM angle and recording the response of all the WFSs. By using the calibrated angular drives we can cast the WFS responses in physical units of ct/urad. The result is shown in Table 3 where the expected dominant terms are shown in blue. For simplicity, the elements a factor of 3 lower than the row dominant term have been omitted.

| | **ΔETM [ct/urad]** | **ΔITM [ct/urad]** | **<ETM> [ct/urad]** | **<ITM> [ct/urad]** | **RM [ct/urad]** |
|---|---|---|---|---|---|
| WFS1 | +13600<br>-14300 | +7500<br>+7200 | | | |
| WFS2A | | | | +14400<br>-13300 | -14000<br>-13900 |
| WFS2B | | -2600<br>+2900 | | -1100(?)<br>+7900(?) | +1000(?)<br>+8540(?) |
| WFS3 | | | -80<br>-80 | <br>+70 | <br>+40 |
| WFS4 | | | +40<br>+40 | -50<br>+40 | +140<br>+120 |

**Table 3: The WFSs response to the different angular DOF measured at 9Hz. In blue are the expected dominant terms. Data: ../scripts/WFS4k/Data/pitH1_03sep29.txt and yawH1_03sep29.txt.**

A few observations:

1. the responses of WFS3 and WFS4 seem not to be well separated (90deg Gouy phase separation, see Table 1). The Gouy phase telescopes on ISCT1 may have to be visited even though the e2e simulation group has shown how the interference of the resonant sidebands with the non-resonant ones generate the observed cross-terms (see G030266);
2. the response of WFS3 and WFS4 have a very low sensitivity with respect to the other WFSs introducing systematic alignment errors; for this reason, the increase of the NR sidebands modulation depth should be considered;
3. the WFS2 demodulation phase has been observed to wonder from day-to-day. This causes the <ITM> and RM signals to leak to WFS2B (Q) with a magnitude comparable to its ΔITM response. To get around this problem, the signal from WFS2B is used to feedback ΔITM with very low gain;
4. the WFS2 demodulation phase has been seen to rotate as the IFO is heated (right after lock acquisition, the laser power is increased from 0.8W to 2.3W to improve the mode-matching of the PRC to the incoming laser beam). The rotation, determined by monitoring an RM pitch line in WFS2B, was initially estimated to be ~100deg (from the *cold* state to the *warmer* state). It was also observed how

the SNR for the ΔITM response significantly dropped making its signal unusable. To get around these problems, we modified its Gouy phase slightly (20deg?) and we were able to decrease the phase rotation down to ~30deg while preserving the ΔITM response;

5. the sensing matrix here reported was measured at one frequency – 9Hz – out of the band of the loop. We verified that the sensing response is flat by measuring it at 18Hz and accounting for the 12dB/octave roll-off due to the suspension.

The control matrix in use is diagonal (despite the non-diagonal sensing matrix) and we use the sensing matrix in Table 3 to calibrate the error points.

| Channel name (H1:ASC-) | Calibration @ 9Hz [ct/urad] | Angular DOF |
|---|---|---|
| WFS1_QP<br>WFS1_Q_PIT | +13600 | ΔETM |
| WFS1_QY<br>WFS1_Q_PIT | -14300 | |
| WFS2_IP<br>WFS2_I_PIT | +14400 | <ITM> |
| WFS2_IY<br>WFS2_I_YAW | -13300 | |
| WFS2_QP<br>WFS2_Q_PIT | -2600 | ΔITM |
| WFS2_QY<br>WFS2_Q_YAW | +2900 | |
| WFS3_IP<br>WFS3_I_PIT | -80 | <ETM> |
| WFS3_IY<br>WFS3_I_YAW | -80 | |
| WFS4_IP<br>WFS4_I_PIT | +140 | RM |
| WFS4_IY<br>WFS4_I_YAW | +120 | |

**Table 4: Calibration of the WFS error points; Channels in green indicate channels stored in Frames.**

In Figure 2-5 we plot the Amplitude Spectral Density (ASD) of the 5 WFS error points calibrated using Table 4. All error points are limited by dark noise above about 50Hz as shown in Figure 3. By looking at the plot in Figure 2, the sensing noise on WFS1 is above the requirement 1e-14 rad/rHz above 40Hz. The residual angular ΔETM fluctuations are below the 1e-8 rad-rms requirement.

Very little effort has been given to decrease the sensing noise and noise reduction will be first addressed after S3. By addressing

- the WFS RF gain;
- the modulation depth for WFS3 and WFS4;
- the whitening gain and filtering;
- the WFS sensing noise

we should be able to significantly reduce the observed sensing noise.

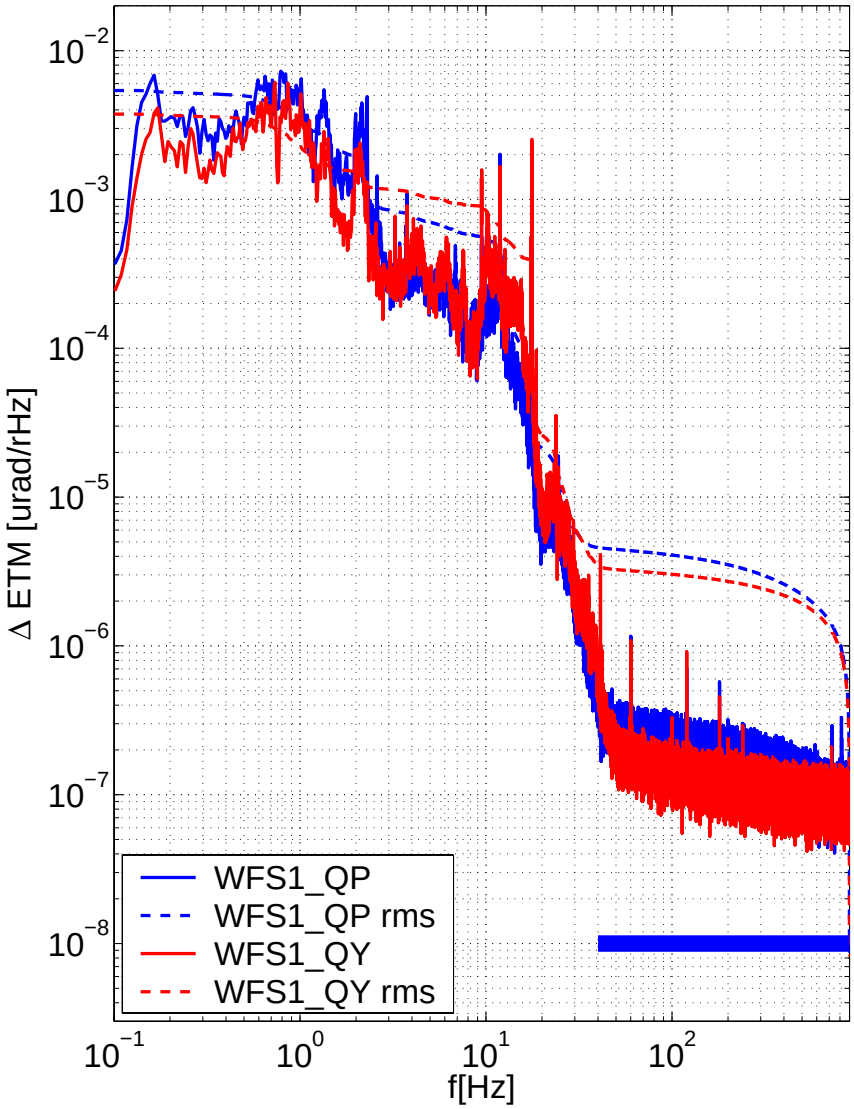


**Figure 2: ASD of the WFS1 error point, in closed loop, with feedback to ΔETM;**

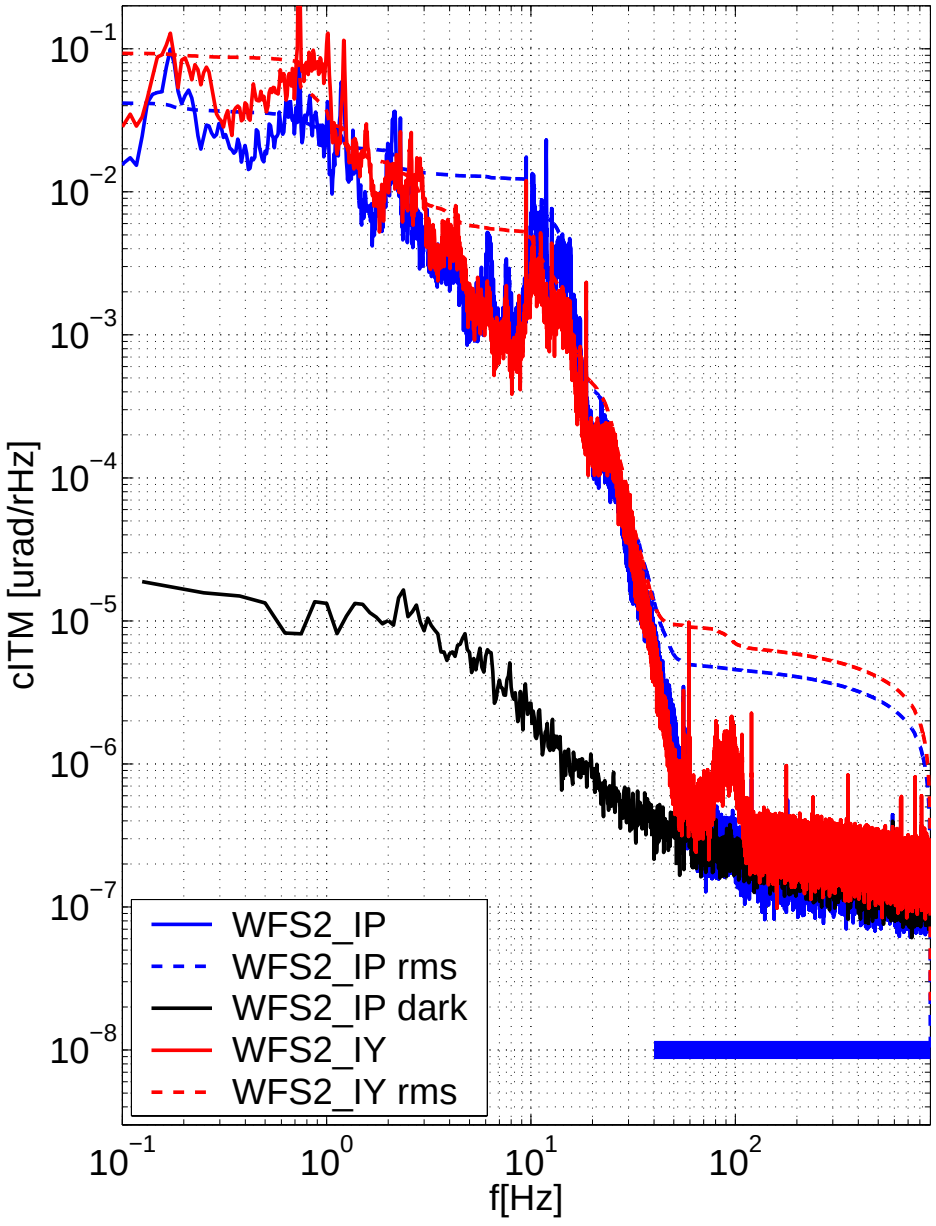


**Figure 3: ASD of the WFS2_I(WFS2A) error point, in closed loop, with feedback to <ITM>.**

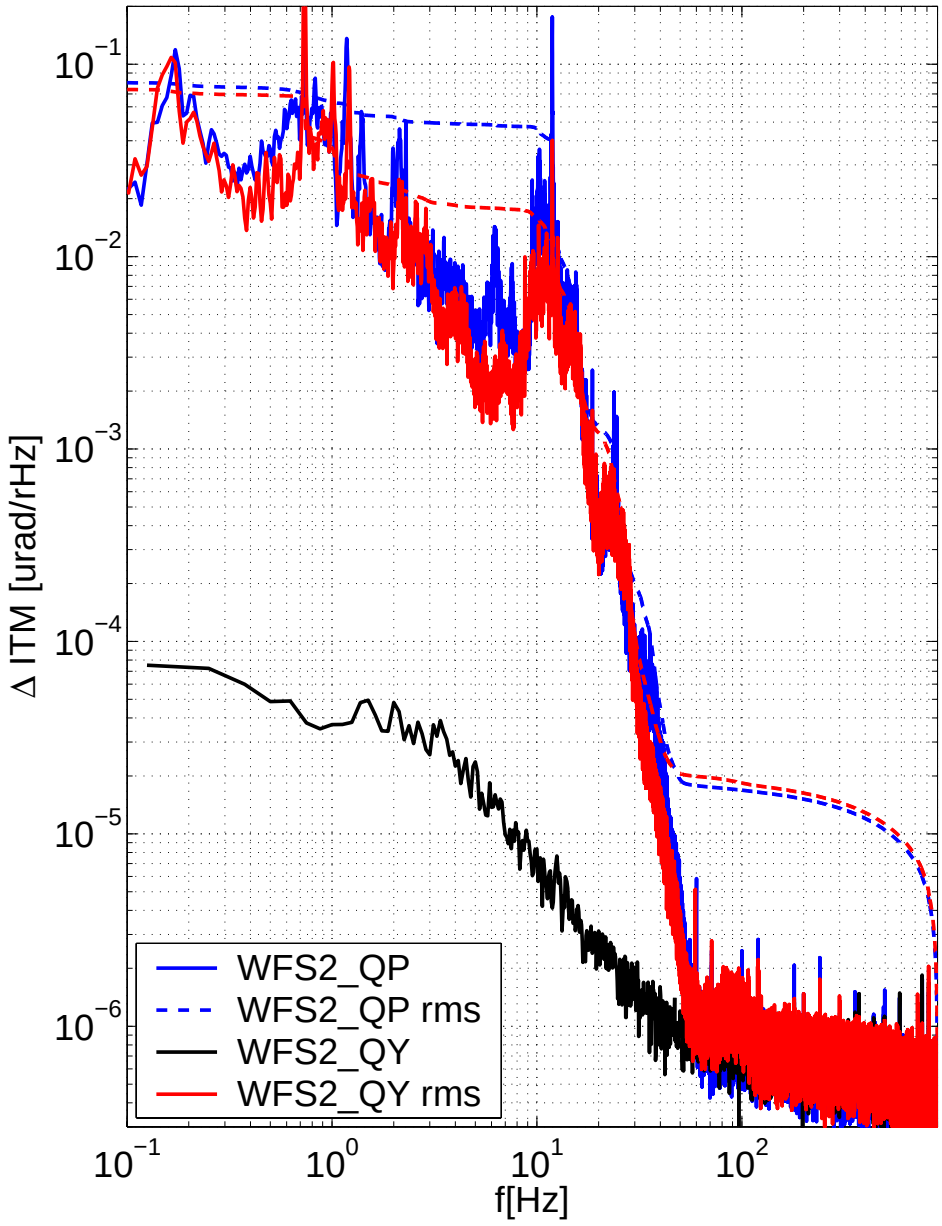


**Figure 4: ASD of the WFS2_Q(WFS2B) error point, in closed loop, with feedback to ΔITM.**

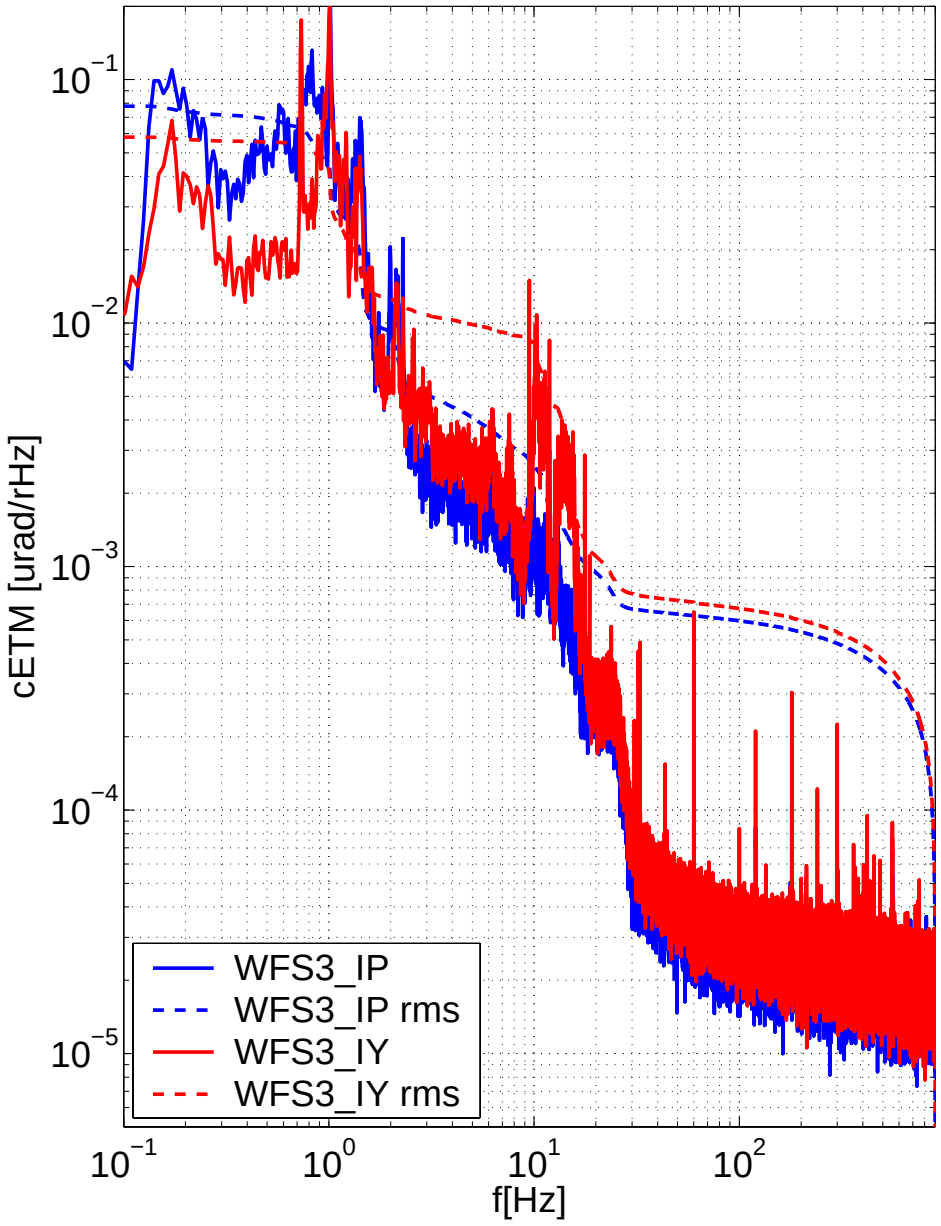


**Figure 5: ASD of the WFS3 error point, in closed loop, with feedback to <ETM>.**

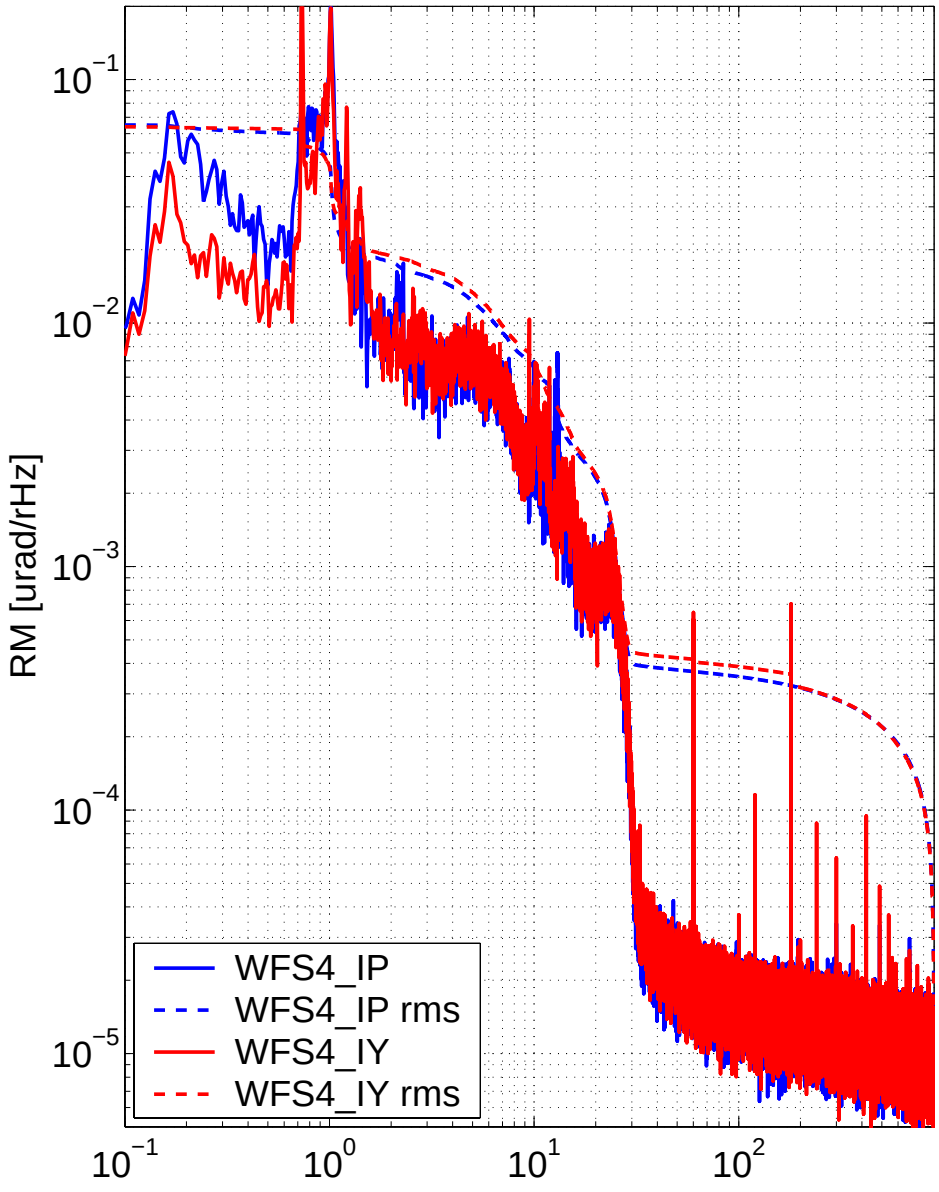


**Figure 6: ASD of the WFS4 error point, in closed loop, with feedback to the RM.**

## THE CONTROL TOPOLOGY

We are currently operating with a diagonal control matrix despite a non-diagonal sensing matrix, which can generate angular instabilities if the gain is not kept *low*. The control topology is summarized in Table 5 where the elements simply denote an amplification factor.

| | WFS1 | WFS2A | WFS2B | WFS3 | WFS4 |
|---|---|---|---|---|---|
| ΔETM | **0.05** | | | | |
| ΔITM | | | **0.35** | | |
| <ETM> | | | | **0.05** | |
| <ITM> | | **0.35** | | | |
| RM | | | | | **0.05** |

**Table 5: The control matrix that rotates the WFS basis in the canonical TM one.**

The filtering involved for each WFS loop is straightforward, consisting of 2 complex zeros to cancel the pendulum roll-off and a pole at 1uHz for stability.

Present in the WFS digital filter banks are also filters to compensate for the OL local damping, which if properly compensated, would make the ASC servo system unconditionally stable for frequencies below 30Hz where the low pass cutoff is placed (see Figure 9).

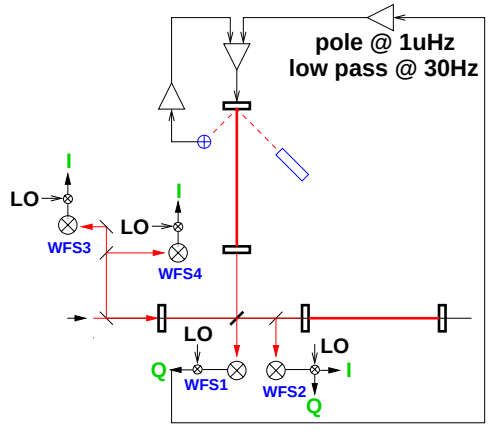


**Figure 9: Simplified diagram of the control scheme.**

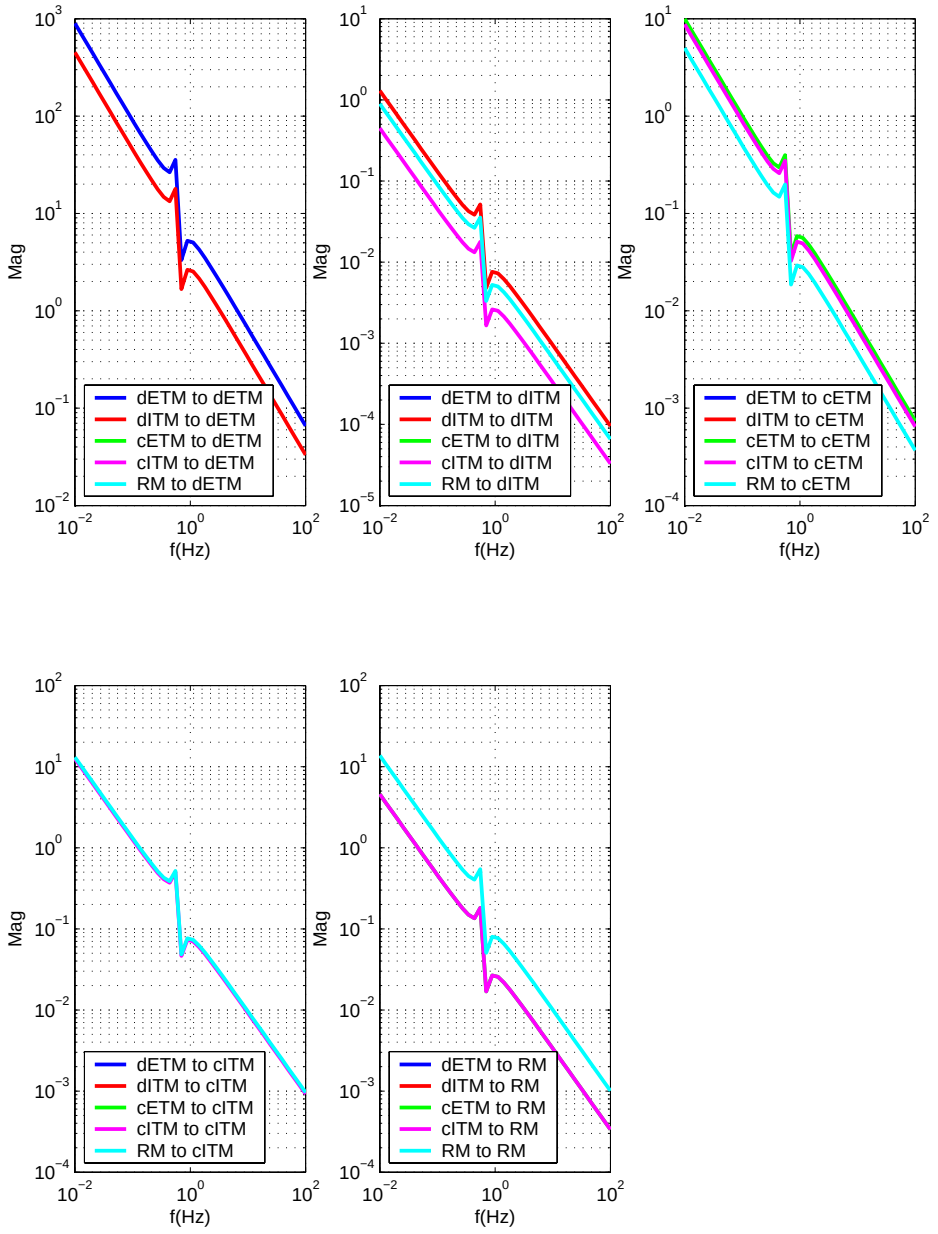


**Figure 10: The TF magnitude of the sensing matrix S, the digital control matrix H and the output matrix C product as a function of frequency. The loop gains were adjusted to fit the measured UGFs.**

The non-diagonal nature of the sensing matrix (Table 3) generates servo instabilities if the WFS cross talk is not addressed in some way. We can quantify this by multiplying the sensing matrix S with the digital control matrix G and the output matrix H (adjusting G so as to obtain the measured Unity Gain Frequencies (UGF)) and this is shown in Figure 10. To get around the servo instabilities, we introduced an hierarchical control system. The loop bandwidths are

- WFS1: typically to a few Hz;
- WFS2A, 3, and 4: hundreds of mHz;
- WFS2B: tens of mHz.

Most of the angular fluctuations originate at the pendulm eigenfrequencies and the ASC system is currently not capable in covering that frequency region (apart from the WFS1 loop). However, by keeping the IFO in the aligned state (with a time constant of a few seconds), we can benefit from the fact that the IFO becomes second-order sensitive to the 1-Hz angular fluctuations. This can be seen in Figure 7 where the left figures plot the arm power (top with ASC off, bottom with ASC on) and the right figures plot the dark fringe light levels (top with ASC off, bottom with ASC on). We can compare

1. how the arm powers are much more stable with the ASC system enabled (full x-axis scale is ~10 hours);
2. how the min-max fluctuations in the AS light level increase as the IFO drifts away from alignment in the uncontrolled case.

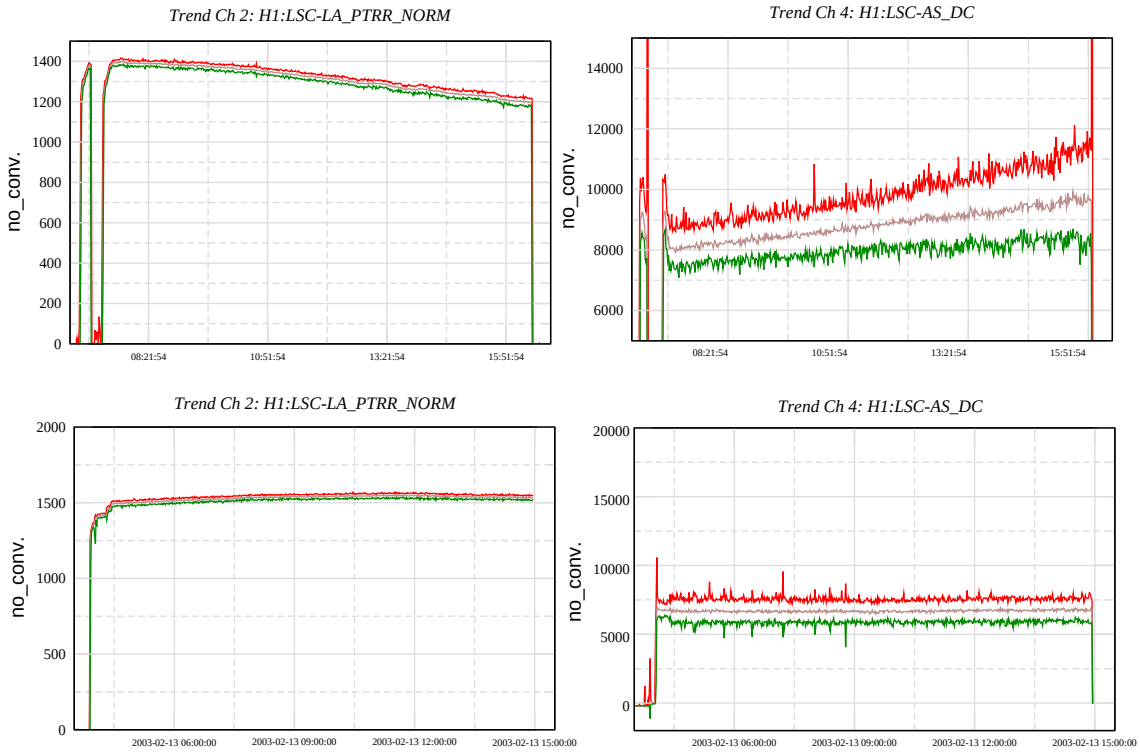


**Figure 7: Top graphs: arm power on transmission (left) and light level at the AS port (right) with no angular control; Bottom graphs: arm power (left) and AS port light with angular control (data taken one week before the S2 run start).**

For the input beam pointing control, the light beams on transmission are collected on Quadrant Photodiodes (QPDs), which give up/down and left/right signals proportional to the beam position on the ETMs. These signals are then used as error signals to center the beam on the ETMs by acting on the BS and MMT3.

## THE ANGULAR-TO-LENGTH COUPLING

By dithering an angular DOF and measuring the L. control point (H1:LSC-DARM_CTRL) we can estimate the angle-to-length coupling for each angular DOF. Table 6 summarizes the results obtained in a lock stretch with the IFO in a nominal configuration. It is worth making the following observations:

1. the coupling coefficients for ITMX and ITMY are very similar indicating that the level of beam centering is about the same;
2. the coupling coefficient for ETMX is a factor of ~3 higher than the one for the ITMs;
3. the ETMY pitch coupling coefficient is significantly lower than the other.

To estimate the angular noise coupling to $H_1$'s displacement sensitivity, we multiplied the ASD of ASCYAW(PIT)_OUT to get to the equivalent length noise. This is shown in Figure 8, which shows that the WFS noise limits the displacement sensitivity in the 20-30Hz region.

| | ETMX [ct/ct] | ETMY [ct/ct] | ITMX [ct/ct] | ITMY [ct/ct] |
|---|---|---|---|---|
| H1:LSC-DARM_CTRL / ASCYAW_OUT | 5.1e-2 | 2.9e-2 | 1.6e-2 | 1.3e-2 |
| H1:LSC-DARM_CTRL / ASCPIT_OUT | 5.7e-2 | 3.6e-3 | 1.3e-2 | 1.0e-2 |

**Table 6: The uncalibrated angle-to-length coupling terms**

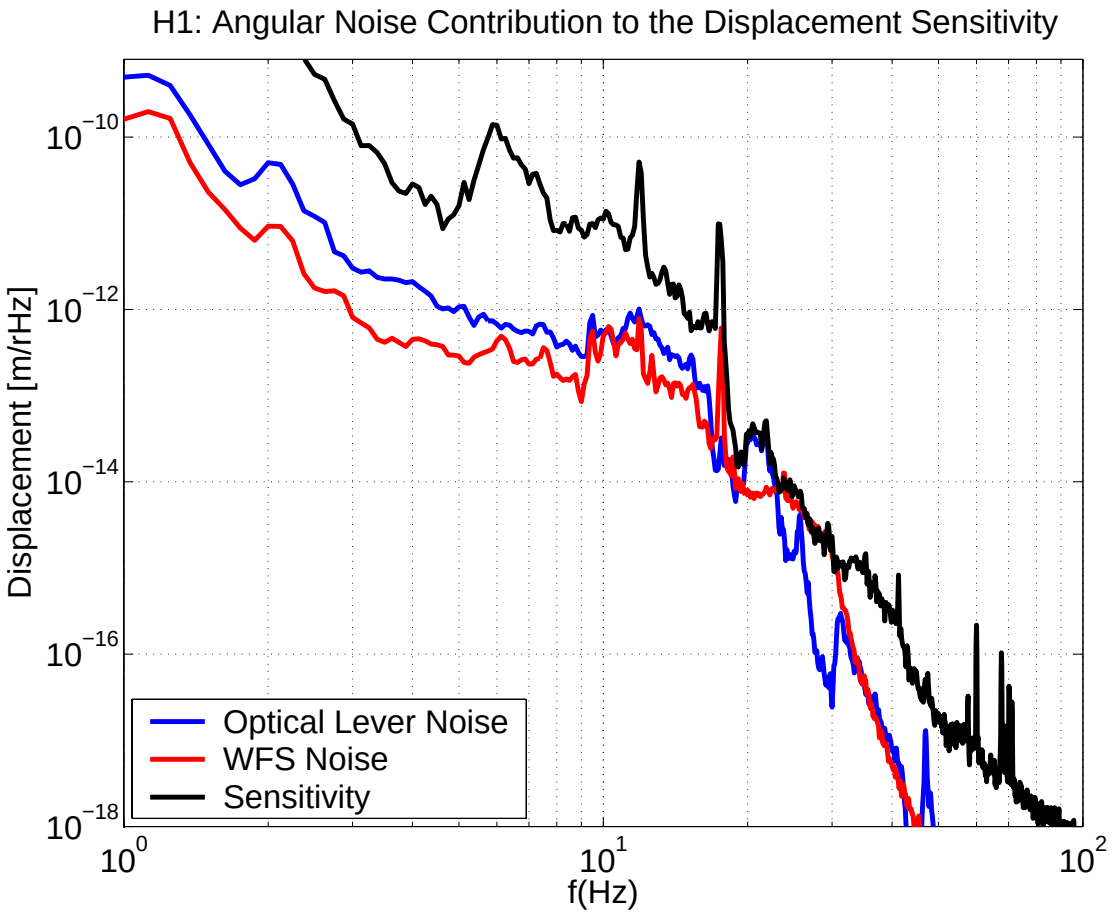


**Figure 8: The angular noise contribution of the Ols and WFSs to the displacement sensitivity of H1; Black: the displacement sensitivity; Blue: the contribution from the Ols; Red: the contribution from the WFS noise.**

**BEAM POSITIONING ON WFS HEAD**

In order to quantify the coupling mechanism between beam position on the WFS and its demodulated signal, we recorded the time series of its DC asymmetry reading (the up/down and left/right DC differences) and its corresponding error point. A plot of the asymmetry vs. its demodulated signal would reveal the presence of a possible correlation.

Figure 11 and 12 show the correlation plot for WFS1 and WFS3 for a lock stretch during E10. There is a linear dependence between the beam position and its error points. There are two possible explanations:

1. Uncontrolled 1Hz angular motion causes both the output beam to shift as well as the demodulated signal to assume a non-zero value. In this scenario, the effect should be significantly reduced once the ASC is able to cover the 1Hz region.
2. In another scenario, the output beam could be dithered in angle by an outside source (not coming from the IFO). This outside modulation would then cause a modulation in the error point.

The second scenario is the most of concern for it would require us to feedback on beam position as well.

Assuming the worst-case scenario and using the calibrations in Table 4, we obtain

- WFS1 pitch: 552/13600*1e-6*asy [rad] = 4e-8 * asy [rad];
- WFS1 yaw: 314/14300*1e-6*asy [rad] = 2e-8 * asy [rad];
- WFS3 pitch: 80/80*1e-6*asy [rad]= 1e-6*asy [rad];
- WFS3 yaw: 65/80*1e-6*asy [rad]=8e-7*asy [rad].

For an asymmetry asy of 10%, WFS1 would introduce an alignment error to the ETMs of 0.4e-8rad, a factor of 2 lower than the 1e-8 rad-rms alignment requirement. Of more concern is the systematic error contribution of WFS3, which for an asymmetry of 10% would produce an unacceptable offset of the order of 1e-7 rad sent to the RM. Similar results were produced for WFS2 and WFS4.

To rule out the worst-case scenario, the transfer function between the WFS error point and an angular dithering generated on the table itself needs to be measured.

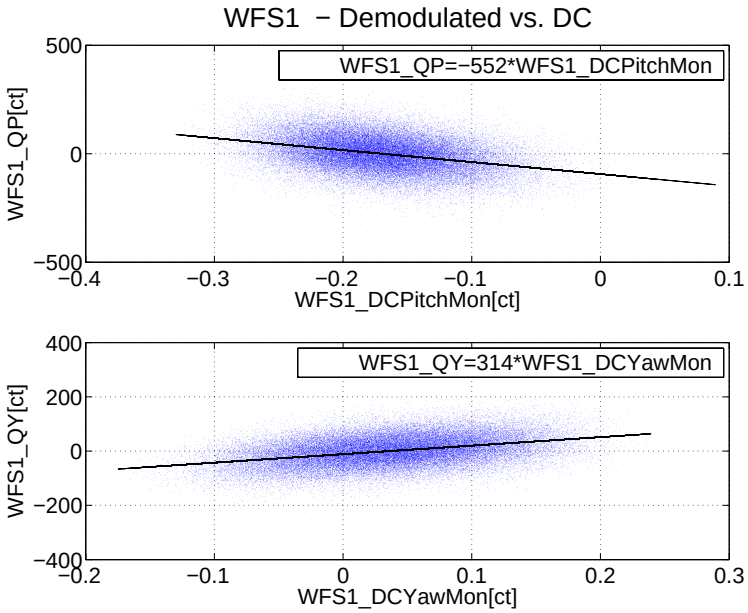


**Figure 11: Correlation plot of WFS1's DC asymmetry and its error points.**

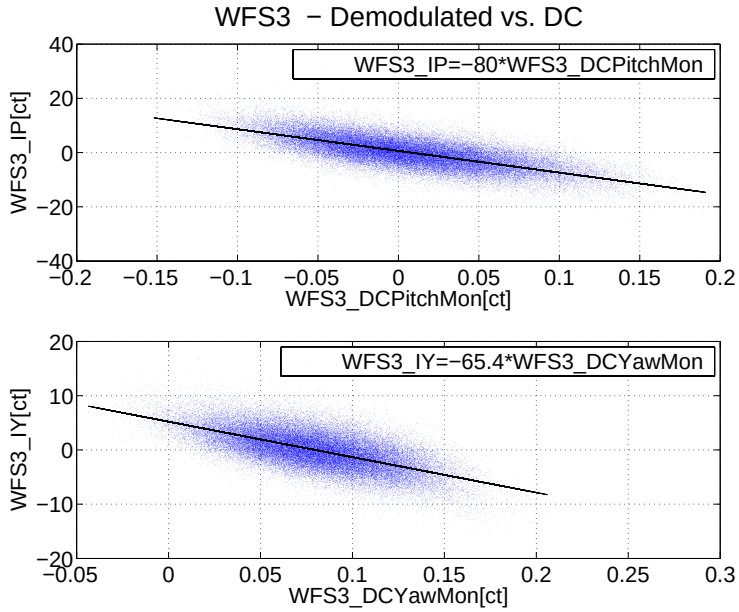


**Figure 12: Correlation plot of WFS3's DC asymmetry and its error points.**